AIP | Journal of Applied Physics

Phenomenological study of barrier imperfection and interfacial scattering on MgO based tunnel junctions

B. J. Chen and S. G. Tan

Citation: Journal of Applied Physics **115**, 034507 (2014); doi: 10.1063/1.4862310
View online: http://dx.doi.org/10.1063/1.4862310
View Table of Contents: http://scitation.aip.org/content/aip/journal/jap/115/3?ver=pdfcov
Published by the AIP Publishing

Phenomenological study of barrier imperfection and interfacial scattering on MgO based tunnel junctions

B. J. Chen[1,a)] and S. G. Tan[1,2]
[1]*Data Storage Institute, A*STAR (Agency for Science, Technology and Research), DSI Building, 5 Engineering Drive 1, Singapore 117608*
[2]*Computational Nanoelectronics and Nano-device Laboratory, National University of Singapore, Singapore 117576*

(Received 6 August 2013; accepted 3 January 2014; published online 16 January 2014)

We investigate the barrier imperfection and interfacial scattering effects on resistance-area product (RA) and tunneling magnetoresistance (TMR) of magnesium oxide (MgO) based magnetic tunneling junction (MTJ). We assume that barrier imperfection reduces the band gap of MgO; thus, it affects both TMR and RA values. The lattice mismatch between MgO and magnetic electrodes leads to interface scattering which reduces TMR. As an application, the MTJ two-state resistance variations due to the process variations are also discussed in the paper. © *2014 AIP Publishing LLC*. [http://dx.doi.org/10.1063/1.4862310]

I. INTRODUCTION

The magnetic tunneling junction (MTJ) is the fundamental building element of the spin-torque transfer magnetic random access memory (STT-MRAM) which is a promising candidate for future memory applications due to its non-volatility, unlimited endurance, high speed, low power, and high scalability.[1–6] An MTJ consists of two ferromagnetic layers (a free layer and a reference layer) separated by a thin tunneling dielectric film. The magnesium oxide (MgO) is currently being used as the tunneling barrier due to its capability of achieving high tunneling magnetoresistance (TMR) for the MTJ.[7–12]

Achieving a high TMR ratio in MgO-based MTJs requires epitaxial growth of the MgO layer with a correct crystalline orientation on ferromagnetic electrodes. Lattice mismatch at the interface and imperfections in the MgO barrier induced during the deposition of MTJs are important factors affecting the resistance-area product (RA) values and TMR ratios. The properties of the thin MgO insulator layers are crucial to the performance of the STT-MRAM. Experimental studies[8] show that barrier imperfections, such as, disorder, defect, and lattice mismatch, alter the band gap of MgO and the tunneling mechanisms (e.g., coherent tunneling and incoherent tunneling), hence affect the TMR and RA values of MTJ.

For MgO-based crystalline MTJ system, the symmetry of the tunneling states at the interfaces is crucial for generating spin current. The Bloch-wave function needs to be considered to reflect the periodicity of the lattice and the matching at the interfaces. The Bloch waves can be calculated by using the layer Korringa-Kohn-Rostoka (LKKR) method based on the density functional theory (DFT).[13–17] The tunneling current can then be computed using the Landauer theory.[18,19] The *ab initio* calculation is extremely useful for the interpretation of experimental results; however, it is very time-consuming.

Eames and Inkson[20] proposed a simplified model which incorporates the effect of interface scattering on TMR for the Fe(001)/MgO(001)/Fe(001) junctions. The interface scatters electron into various channels, linking electron transport to the complex band structure of the MgO. We found that this model is particularly suitable for a simple adaption to account for more realistic interfacial and barrier effects.

In this paper, we first present an expanded version of Eames' model to calculate the voltage dependent tunneling conductance and TMR of the MgO-based MTJ by introducing phenomenological parameters to the Eames's model to include the effects of interface scattering and barrier imperfection; then, we examine the effects of barrier imperfection and interface condition on RA and TMR of MgO based MTJ by various parameters combinations. Finally, the MTJ resistance variations due to the process variations are discussed for a specific MTJ.

II. TUNNELING MODEL FOR MGO(001) BASED MTJ SYSTEMS

Figure 1 is the schematic of an MTJ device with applied bias V and barrier thickness d. The carrier in the left electrode with bandwidth E_{F1} can tunnel into the right electrode with bandwidth E_{F3} under an applied bias V. The transmission coefficient T in this case can be determined by solving the Schrödinger equation in the three regions of the MTJ. The results can be expressed as[20]

$$|T|^2 = \frac{16m_2^2/m_1^2k_\perp^2\gamma(k,V,0)\gamma(k,v,d)\exp\left[-2\int_0^d\gamma(k,V,x)dx\right]}{[k_\perp^2m_2^2/m_1^2+\gamma^2(k,V,0)][q_\perp^2m_2^2/m_3^2+\gamma^2(k,V,d)]}, \quad (1)$$

where

$$\gamma^2(k,V,x) = k_{||}^2 + m_2/m_1\left(k_0^2 - k_{||}^2 - k_\perp^2 - \frac{x}{d}k_V^2\right) \quad (2)$$

and

[a)]Author to whom correspondence should be addressed. Electronic mail: Chen_BingJin@dsi.a-star.edu.sg

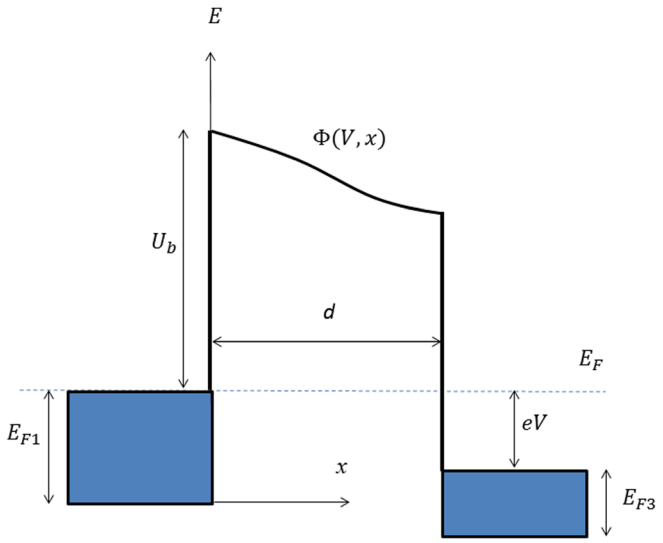

FIG. 1. Schematic of an MTJ with the relevant potential parameters and bandwidths.

$$q_\perp^2 = m_3/m_1(k_\perp^2 + k_V^2) + \frac{2m_1}{\hbar^2}(E_{F1} - E_{F3}). \tag{3}$$

In the above equations, k ($k^2 = k_{||}^2 + k_\perp^2$) is the wave vector of the incident electron, V is the applied voltage, d is the thickness of the MgO barrier; m_1, m_2, and m_3 are the effective masses in the left electrode, the barrier, and the right electrode, respectively. $k_\perp$ ($k_{||}$) is the component of the effective wave vector of the electron perpendicular (parallel) to the barrier in the left electrode. $q_\perp$ is the component of the effective wave vector of the electron perpendicular to the barrier in the right electrode. k_V and k_0 are the effective wave vectors due to the applied voltage and the barrier height, respectively, i.e.,

$$k_0^2 = \frac{2m_1 U}{\hbar^2}, \quad k_v^2 = \frac{2m_1 eV}{\hbar^2}, \tag{4}$$

where $U = U_b + E_{F1}$ is the potential of the barrier.

The tunneling current density J corresponding to the tunneling channel at zero temperature as a function of the applied voltage V, can be computed by using quantum mechanics theory[21]

$$J(V) = \frac{e\hbar}{2m_3} i(\Psi\nabla\Psi^* - \Psi^*\nabla\Psi), \tag{5}$$

which leads to

$$J(V) = \frac{e\hbar}{4\pi^2 m_3}\left[\int_0^{\sqrt{k_F^2 - k_V^2}} k_{||}dk_{||}\int_{\sqrt{k_F^2 - k_{||}^2 - k_V^2}}^{\sqrt{k_F^2 - k_{||}^2}} q_\perp |T|^2 dk_\perp + \int_{\sqrt{k_F^2 - k_V^2}}^{k_F} k_{||}dk_{||}\int_0^{\sqrt{k_F^2 - k_{||}^2}} q_\perp |T|^2 dk_\perp\right]. \tag{6}$$

Here, $k_F^2 = \frac{2m_1 E_{F1}}{\hbar^2}$. The conductance is calculated from $G = dJ/dV$, and the RA value is $RA = dV/dJ$.

For the Fe(001)/MgO(001)/Fe(001) junctions, at the Fermi level, the majority spin electrons are associated with the Δ_1, $\Delta_{2'}$, and Δ_5 bands in the electrode, while the minority spin electrons are associated with the Δ_2, $\Delta_{2'}$, and Δ_5 bands. In the MgO barrier, the energy bands are of Δ_1, Δ_2, and Δ_5 symmetry. However, only the Δ_1 band forms the tunneling channel since the decay rate within the barrier is much less for the other two bands.[13,14]

The *ab initio* calculation indicates that for parallel magnetic alignment, the conductance $G^{\uparrow\uparrow}$ is significant. It is related to the majority spin electrons in the Δ_1 band of the left electrode. These electrons match onto the MgO(001) Δ_1 complex band and tunnel directly into the Δ_1 band in the right electrode. However; contribution from the minority spins ($G^{\downarrow\downarrow}$) can be neglected since the minority spins arise primary from the Δ_5 band in the electrode, which decays much faster within the MgO barrier. For anti-parallel magnetic alignment, the conductance $G^{\downarrow\uparrow}$ is small since there is no Δ_1 state in the left electrode. The conductance $G^{\uparrow\downarrow}$ is also small because the majority spin from the left electrode cannot propagate in the minority spin channel in the right electrode. The device acts like a spin filter where current in the parallel configuration is much greater than current in the anti-parallel configuration, resulting in a very large TMR. However, experimental studies always show much lower TMR due to the interface imperfection of the MTJ in the real experiment.

We introduce the following transmission coefficient matrix, to describe the tunneling probability between various bands through the MTJ:

$$T_s = \begin{bmatrix} T_{11} & cT_{15} \\ cT_{51} & c^2T_{55} \end{bmatrix}, \tag{7}$$

where $T_{ij}(i,j = 1,5)$ is the transmission coefficient when electrons tunnel from Δ_i in the left electrode to Δ_j in the right electrode. The parameter c is the probability of the minority spin Fe(Δ_5) tunneling into MgO(Δ_1), which is given by

$$c = S_0 k_{||}, \tag{8}$$

where S_0 is a function of the complex wave vector band gap and effective masses of the conduction and lighthole bands.[20]

In order to include the effects from both the strength of interface scattering and the barrier imperfection, we introduce two additional parameters to the Eames's model. First, the transfer probability in Eq. (8) is modified to

$$c = c_s S_0 k_{II}, \tag{9}$$

where the parameter c_s is introduced to account for the different scattering strengths due to interface imperfection. Hence, smaller c_s indicates better interface, resulting in larger TMR. Second, the barrier height is assumed to be

$$U_b = c_b \frac{E_g}{2}, \tag{10}$$

where the parameter c_b is introduced to reflect the barrier height reduction due to the defects in MgO.[22] Here, E_g is the band gap of the ideal bulk MgO.

III. FITTING PARAMETERS WITH EXPERIMENTAL RESULTS

We use this model to fit the parameters c_s and U_b with the experimental results conducted by Yuasa *et al.* for the Fe(001)/MgO(001)/Fe(001) MTJ systems.[22]

In the experiment, RA value is about 8800 $\Omega\,\mu m^2$ and TMR ratios are 180% at 293 K and 247% at 20 K for $d = 2.3$ nm at a bias voltage of 10 mV. To compare it with our theoretical model, we need the experimental results for T = 0 K. To do this, we make use of a temperature dependent model[23–25] which is described by

$$G_P(T) = G_0[1 + P_0^2(1 - \alpha T^{1.5})^2], \tag{11}$$

$$G_{AP}(T) = G_0[1 - P_0^2(1 - \alpha T^{1.5})^2], \tag{12}$$

where α is a material-dependent constant, P_0 is the full effective spin polarization at $T = 0$K, and G_0 is assumed to be constant. The fitted parameters are $c_s = 1.35$ and $U_b = 1.30$ eV.

It should be noted that, the fitted potential barrier height with our modified model (1.30 eV) is much higher than that achieved using Simmons' model (0.4 eV).[26] The value from our model is lower than the ideal bulk MgO barrier height 3.75 eV.[27] This could be due to the presence of oxygen vacancies defect in the realistic MgO used in the experiment.

IV. EFFECTS OF BARRIER IMPERFECTION AND INTERFACE CONDITION ON RA AND TMR

We use this model to study how the barrier imperfection and the interface affect the RA and TMR of Fe(001)/MgO(001)/Fe(001) MTJ systems. In the simulations, the Fermi width of the Δ_1 Fe(001) band is 1 eV and the effective mass is 1 m_e; the Fermi width of the Δ_5 Fe(001) band is 0.45 eV and the effective mass is 2.3 m_e; the effective mass of the MgO is 0.35 m_e.[9,28] The barrier height U_b is assumed to be varied with MgO thickness d according to Eq. (13), where c_b is a parameter to be fitted with experiment

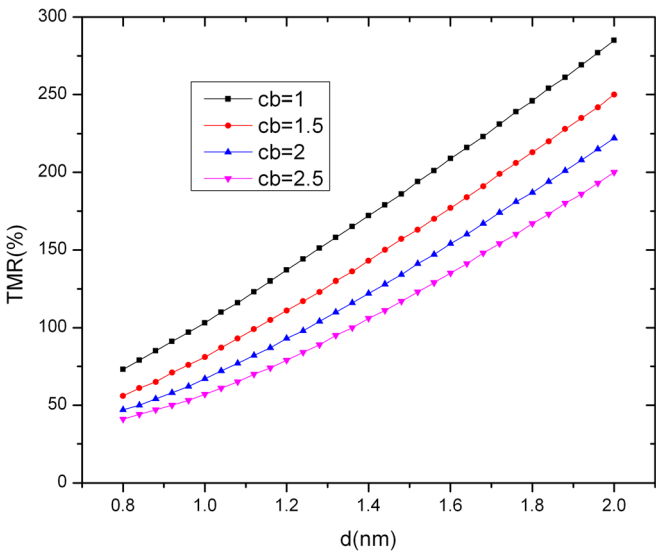

FIG. 2. Dependence of TMR on MgO thickness for different fitting parameters c_b ($c_s = 1.5$).

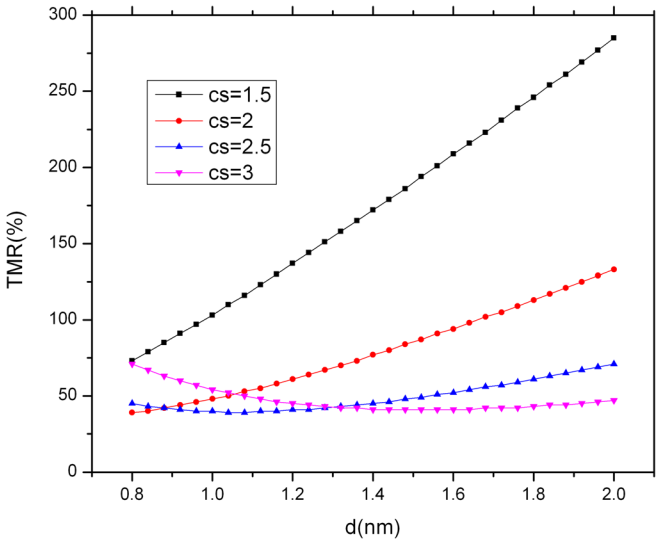

FIG. 3. Dependence of TMR on MgO thickness for different fitting parameters c_s ($c_b = 1.0$).

results. The Fermi level of the system is assumed to be in the middle of the band gap of the barrier.

$$U_b = \frac{E_g}{2}\frac{d}{d + c_b}. \tag{13}$$

By using Eq. (13), we assume that the barrier height of the realistic MgO increases with increasing barrier thickness and approach $E_g/2$ for thick barrier. This is consistent with the experimental evidence,[8] where the author attributes the decrease in barrier height with thinner MgO thickness as arising from an increase in disorder and defect density due to the strong compressive stress at the interface.

Figure 2 shows that TMR increases with increasing MgO thickness at $c_s = 1.5$ for all different c_bs. Smaller c_b indicates higher U_b, which improves TMR. Figure 3 shows that c_s has significant effect on the TMR behaviors. For weak interface scattering (smaller c_s), the symmetry

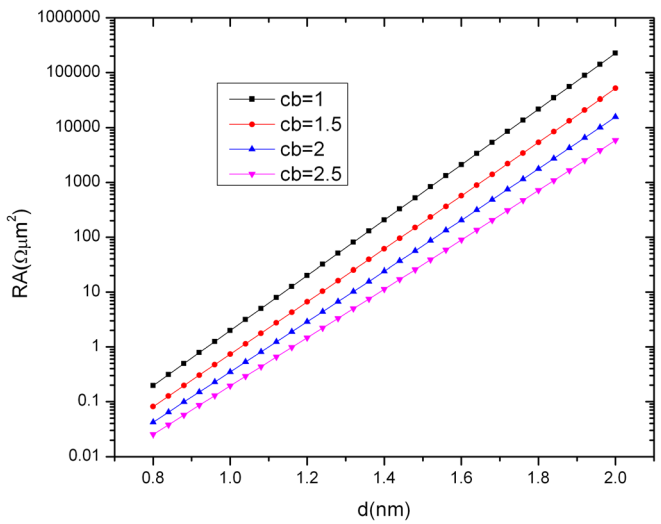

FIG. 4. Dependence of RA on MgO thickness for different fitting parameters c_b ($c_s = 1.5$).

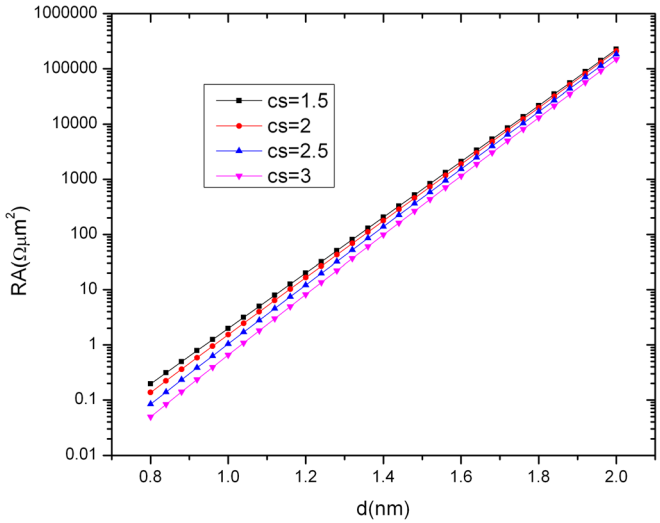

FIG. 5. Dependence of RA on MgO thickness for different fitting parameters c_s ($c_b = 1.0$).

effect at the interface takes into effect, the spin filtering efficiency increases with increasing barrier thickness, resulting in TMR increasing with increasing MgO thickness. However, TMR decreases with increasing MgO thickness for strong interface scattering (larger c_s). This is because the symmetry at the interface breaks, resulting in TMR performance similar to the amorphous barrier. The dependence of RA values on the MgO thickness for different c_s and c_b are depicted in Figures 4 and 5.

V. THE MTJ RESISTANCE VARIATIONS DUE TO PROCESS VARIATIONS

The process variations of MTJ, such as barrier thickness and cross-section area, result in MTJ resistance variations, and cause read error. Figures 6–8 show 1σ variation of two-state resistances and TMR, respectively, as a function of c_s or c_b for an MTJ with nominated MgO thickness of 1 nm and cross-section area of 0.001 μm^2. The variations of the

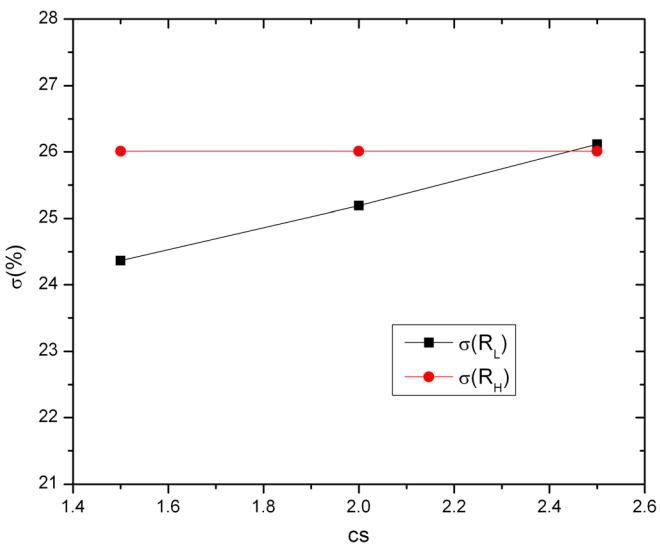

FIG. 6. Standard deviation of two-state resistances as functions of fitting parameter c_s ($d_0 = 1$ nm, $A_0 = 0.001\ \mu$m^2, $\sigma_d = 2\%$, $\sigma_A = 5\%$, and $c_b = 1.0$).

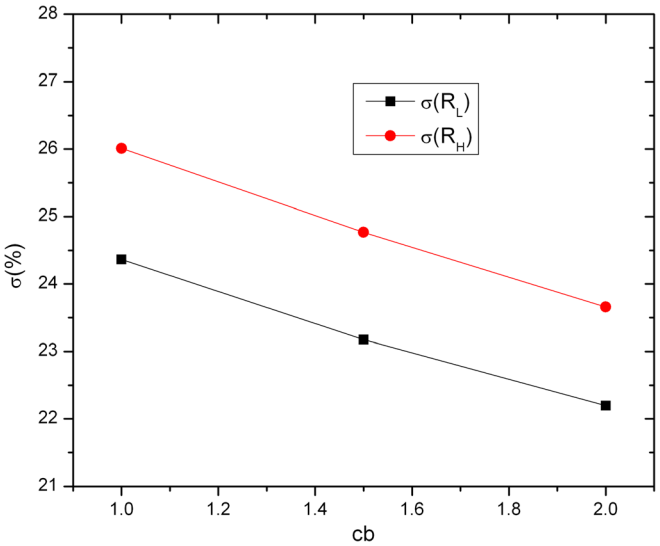

FIG. 7. Standard deviation of two-state resistances as functions of fitting parameter c_b ($d_0 = 1$ nm, $A_0 = 0.001\ \mu$m^2, $\sigma_d = 2\%$, $\sigma_A = 5\%$, and $c_s = 1.5$).

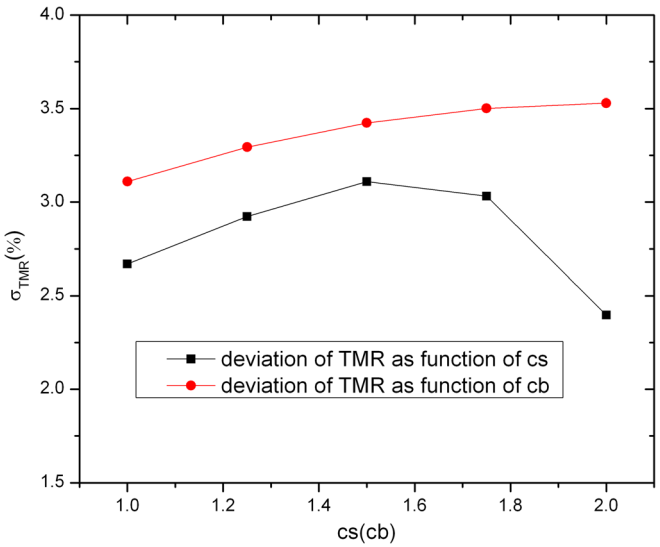

FIG. 8. Standard deviation of TMR as functions of fitting parameters ($d_0 = 1$ nm, $A_0 = 0.001\ \mu$m^2, $\sigma_d = 2\%$, and $\sigma_A = 5\%$).

MgO thickness and MTJ cross-section area are 2% and 5%, respectively. Here, the variations are plotted as the percentage to their mean values. The variations of the MTJ low state resistance (R_L) increase with increasing c_s. However, c_s does not affect the variation of the MTJ high state resistance (R_H). Both $\sigma(R_L)$ and $\sigma(R_H)$ decrease with increasing c_b. Figure 8 shows that the deviation of TMR decreases with decreasing c_b. It first increases then decreases with decreasing c_s. Since TMR value also favorites small c_b and small c_s, small c_b and small c_s help to enhance TMR and reduce its distribution. However, small c_b will increase RA value significantly.

VI. CONCLUSIONS

In summary, we have studied the barrier imperfection and interface conditions on TMR and RA values of MgO-

based MTJ. We have shown that both barrier imperfection and interface conditions affect the RA and TMR significantly. Barrier imperfection reduced band gap of MgO, resulting in reduced RA and TMR. For weak interface scattering, TMR increases with increasing MgO thickness. However; TMR decreases with increasing MgO thickness for strong interface scattering. We have also shown that interface scattering increases the MTJ low resistance (R_L) variations; however, it does not affect the MTJ high resistance (R_H) variations. On the other hand, barrier imperfection reduces both the R_L and R_H variations. In addition, smaller c_b and smaller c_s help to enhance TMR value and reduce its distribution for better performance of TMR device. However, small c_b will increase RA value significantly.

[1]M. Hosomi, H. Yamagishi, T. Yamamoto, K. Bessho, Y. Higo, K. Yamane, H. Yamada, M. Shoji, H. Hachino, C. Fukumoto, H. Nagao, and H. Kano, Tech. Dig. - Int. Electron Devices Meet. **473**, 459 (2005).
[2]Y. Chen, X. Wang, H. Li, H. Xi, W. Zhu, and Y. Yan, IEEE Trans. Very Large Scale Integr. Syst. **18**, 1724 (2010).
[3]Z. Diao, M. Pakala, A. Panchula, Y. Ding, D. Apalkov, L. C. Wang, E. Chen, and Y. Huai, J. Appl. Phys. **99**, 08G510 (2006).
[4]R. Sbiaa, S. Lua, R. Law, H. Meng, R. Lye, and H. K. Tan, J. Appl. Phys. **109**, 07C707 (2011).
[5]H. Zhao, A. Lyle, Y. Zhang, P. K. Amiri, G. Rowlands, Z. Zeng, J. Katine, H. Jiang, K. Galatsis, K. L. Wang *et al.*, J. Appl. Phys. **109**, 07C720 (2011).
[6]M. T. Rahman, A. Lyle, G. Hu, W. J. Gallagher, and J. Wang, J. Appl. Phys. **109**, 07C709 (2011).
[7]W. H. Butler, Sci. Technol. Adv. Mater. **9**, 014106 (2008).
[8]P. G. Mather, J. C. Read, and R. A. Buhrman, Phys. Rev. B **73**, 205412 (2006).
[9]X.-G. Zhang, W. H. Butler, and A. Bandyopadhyay, Phys. Rev. B **68**, 092402 (2003).
[10]D. D. Djayaprawira, K. Tsunekawa, M. Nagai, H. Maehara, S. Yamagata, N. Watanabe, S. Yuasa, Y. Suziki, and K. Ando, Appl. Phys. Lett. **86**, 092502 (2005).
[11]J. D. Burton, S. S. Jaswal, E. Y. Tsymbal, O. N. Mryasov, and O. G. Heinonen, Appl. Phys. Lett. **89**, 142507 (2006).
[12]J. Faure-Vincent, C. Tiusan, E. Jouguelet, F. Canet, M. Sajieddine, C. Bellouard, E. Popova, M. Hehn, F. Montaigne, and A. Schuhl, Appl. Phys. Lett. **82**, 4507 (2003).
[13]W. H. Butler, X. G. Zhang, T. C. Schulthess, and J. M. Maclaren, Phys. Rev. B **63**, 054416 (2001).
[14]W. G. Wang, C. Ni, G. X. Miao, C. Weiland, L. R. Shah, X. Fan, P. Parson, J. Jordan-sweet, X. M. Kou, Y. P. Zhang, R. Stearrett, E. R. Nowak, R. Opila, J. S. Moodera, and J. Q. Xiao, Phys. Rev. B **81**, 144406 (2010).
[15]J. Mathon and A. Umerski, Phys. Rev. B **63**, 220403 (2001).
[16]J. M. MacLaren, X. G. Zhang, W. H. Butler, and X. D. Wang, Phys. Rev. B **59**, 5470 (1999).
[17]X. G. Zhang and W. H. Butler, Phys. Rev. B **70**, 172407 (2004).
[18]R. Landauer, IBM J. Res. Dev. **1**, 223 (1957).
[19]R. Landauer, Philos. Mag. **21**, 863 (1970).
[20]M. E. Eames and J. C. Inkson, Appl. Phys. Lett. **88**, 252511 (2006).
[21]A. S. Davydov, *Quantum Mechanics*, 2nd ed. (Pregamon Press, 1973).
[22]S. Yuasa, T. Nagahama, A. Fukushima, Y. Suzuki, and K. Ando, Nature Mater. **3**, 868 (2004).
[23]X. Kou, Appl. Phys. Lett. **88**, 212115 (2006).
[24]C. H. Shang, J. Nowak, R. Jansen, and J. S. Moodera, Phys. Rev. B **58**, R2917 (1998).
[25]M. EI Baraji, V. Javerliac, W. Guo, G. Prenat, and B. Dieny, J. Appl. Phys. **106**, 123906 (2009).
[26]J. Simmons, J. Appl. Phys. **34**, 1793 (1963).
[27]W. Wulfhekel, M. Klaua, D. Ullmann, F. Zavaliche, J. Kirschner, R. Urban, T. Monchesky, and B. Heinrich, Appl. Phys. Lett. **78**, 509 (2001).
[28]J. Callaway and C. S. Wang, Phys. Rev. B **16**, 2095 (1977).